The 205 MHz ST Radar at Cochin: A National facility to probe the Tropical Atmosphere and Ionosphere

Rejoy Rebello[1], Rakesh. V[1], Sarathkrishna S[1], Titu K Samson [1], Sivan C[1], Abhiram Nirmal C S[1], Manoj. M. G[1], Ajil. Kottayil[1], Syam Sankar[1], Vijaykumar P[1], Sunitha Nair[1], K. Mohankumar[1], P. Mohanan[1], Santosh K R[1], K. Vasudevan[1], K. Satheesan[1] and S. Abhilash[1,*]

[1]Advanced Centre for Atmospheric Radar Research
Cochin University of Science and Technology, Cochin 682022
Email: abhimets@gmail.com

ABSTRACT

The stratosphere–troposphere (ST) Radar at Cochin is the World's first atmospheric wind profiler radar operating at 205 MHz range is an active phased array radar to study the near equatorial atmospheric processes. This wind profiler radar commissioned at Advanced Centre for Atmospheric Radar Research (ACARR), Cochin University of Science and Technology (CUSAT) is designed, developed, and installed indigenously, and hence became the part of the prestigious "Make in India Program" of the Government of India. This project is funded by the Department of Science and Technology, Science Engineering Research Board (SERB) under the Intensification of Research in High Priority Area (IRHPA) scheme of Government of India. The 205 MHz ST radar framework at Cochin is a clear-air active phased array wind profiler radar (WPR) using electronic beam steering of 0-30° off –zenith and 0-360° along azimuth in steps of 1° intervals. The wind profiler uses the Doppler Beam Swinging (DBS) method to analyse the backscattered signals for calculating the Doppler shifts at different heights ranging from 315 m to 20 km in the atmosphere. The turbulence results from refractive index fluctuations due to variations in different atmospheric parameters like temperature, humidity, electron density, etc. The 205 MHz ST radar at Cochin consists of 619 Yagi-Uda antennas arranged in a circular aperture with a diameter of about 27 m. The main advantage of this Radar site is its geographical location, which enables to understand the dynamics of the tropical atmosphere and equatorial ionosphere. In addition, ST Radar operating at 205 MHz has got several advantages over conventional wind profiler radars operating at a lower frequency range of about 40-60 MHz and at higher frequency range of 400 MHz to 1GHz. The 205 MHz ST radars are less affected by cosmic noise and hence the accuracy is better. Unlike the UHF radar in which signals saturates in rainy conditions, the 205 MHz. radar does not. Hence ST radars operating at 205 MHz. is considered as a better trade-off between the 50 and 400 MHz radars in terms of galactic noise, cost effectiveness, physical size of antenna, better vertical resolution, and height coverage, especially over the tropics, where tropopause height is around 15 km. The 205 MHz ST Radar provides high resolution wind information from 315 m to 20 km in all weather conditions, which enables better understanding of the dynamics and physics of the atmosphere and weather systems. Another added advantage of this radar is its capability of exploring space weather activities, ionospheric disturbances, tracking of celestial bodies in the radar vicinity and Radio Astronomical studies. This article describes the technical details, salient features, and application potential of 205 MHz. ST radar at ACARR, CUSAT.

Keywords: *Wind profiler, 205 MHz. ST radar, Signal Processing, Radar Meteorology, Ionospheric Process*.

1. Introduction

Wind profiler radar (WPR), sometimes known as atmospheric radar, is a cutting-edge device that continually monitors horizontal and vertical winds in the troposphere and stratosphere in all weather conditions. The coherent integration at very high frequency (VHF) approach is employed in these radars to identify signal returns caused by minor fluctuations in the atmospheric refractive index. These radars transmit electromagnetic radiation pulses by guiding beams 15 degrees off-zenith in multiple orthogonal directions to calculate the three-dimensional wind vector. A tiny portion of the energy delivered in each direction is backscattered back to the radar. The movement of the scattering medium generates a Doppler shift in the backscatter returns, which are analysed at discrete intervals in the receiver [1] [2].

Depending on the nature of the scattering mechanism, atmospheric radars can operate at a wide range of frequencies in the VHF (30-300 MHz) and near ultra-high frequency (UHF) (300-1400 MHz) bands [2], depending on factors such as location, design, and configuration of the wind profiler system. The selection of the operating frequency is based on specific applications and study requirements, considering the advantages and trade-offs in terms of spatial resolution, range, and sensitivity to different atmospheric phenomena at that location. Lower frequencies utilized in wind profilers offer longer-range coverage but with lower spatial resolution. In contrast, higher frequencies provide higher spatial resolution but shorter-range coverage. These considerations are essential for effectively observing and analyzing the wind patterns and atmospheric dynamics in each area. In a later stage of radar development, 50 MHz radars were explicitly designed to study the vertical structure and dynamics of the Earth's atmosphere, primarily in the mesosphere, stratosphere, and troposphere regions. The lower frequency of 50 MHz allows for extended range coverage and the ability to penetrate deeper into the atmosphere than higher-frequency radars. As a result, it becomes suitable for studying various atmospheric phenomena in the middle and lower layers of the atmosphere. The long wavelength associated with the 50 MHz radar is particularly adept at detecting and analyzing large-scale atmospheric features with enhanced sensitivity. This capability offers valuable insights into the dynamics of the atmosphere over a wide range of altitudes. Near-UHF radars are specifically developed for boundary layer and lower tropospheric research [3]. They are in the 1000 MHz frequency band (30 cm wavelength), commonly known as boundary layer radar, with a typical lowest range gate of around 100 m. The maximum detectable signal changes depending on the atmospheric conditions. The observed altitude typically ranges from 1.5 to 5 km above ground level. The vertical sampling resolution mode ranges from 60 to 100 metres. When compared to lower frequency wind profilers, 1000 MHz wind profiler radars are smaller, less expensive, and easier to transport. Atmospheric radars on the mesoscale system operate at 400 MHz (75 cm wavelength) to meet the needs of the troposphere in terms of vertical range and resolution. They are used to measure and monitor the dynamics of the atmosphere at altitudes ranging from 8 to 12 km. The transmitters on 400 MHz radars are more powerful than those on 1000 MHz radars. These wind profiler radars are inexpensive and convenient tools for meteorological analysis and forecasting. Mesosphere- stratosphere-troposphere (MST) radars are commonly employed for continuous monitoring of three- dimensional wind vector profiles in the highest levels of the atmosphere. In the VHF region, such radars operate at a frequency of roughly 50 MHz (6 m wavelength). These radars conduct continuous observations at altitudes ranging from 2 to 25 kilometres. They can also track intermittent observations spanning 60 to 90 km, as well as the ionospheric E and F regions. MST radars give useful information on dynamical and electrodynamic processes, such as the interaction of the lower atmosphere to the ionosphere [1] [4].

1.1 Uniqueness and advantages of 205 MHz Radar

Figure 1 depicts the many parameters impacting the choice of frequency for WPR stated by Balsley and Gauge [5]. Wind profiler radars were created in the typical frequency ranges of 50, 400, and 1000 MHz, and their advantages and disadvantages are graphically depicted in this picture. The figure's dashed vertical line depicts the 200 MHz band (1.46 m wavelength). The potential of radar operating at 200 MHz for wind profiling is unknown [6]. However, based on NASA's feasibility assessments for monitoring the wind for space shuttle launches, frequencies of 50, 225, and 400 MHz were good enough for exploring stratospheric and tropospheric heights [7]. Previously, no effort had been attempted to come up with wind profiler radar at frequencies close to 200 MHz because this band of frequencies is widely utilised for radio and television broadcasts. Recent broadcasting techniques, however, have shifted from analogue to digital, and the 180-220 MHz frequency ranges are now also available for meteorological investigations. Figure 2 depicts the maximum obtainable height for a fixed value of power aperture product (PAP) as a function of frequency

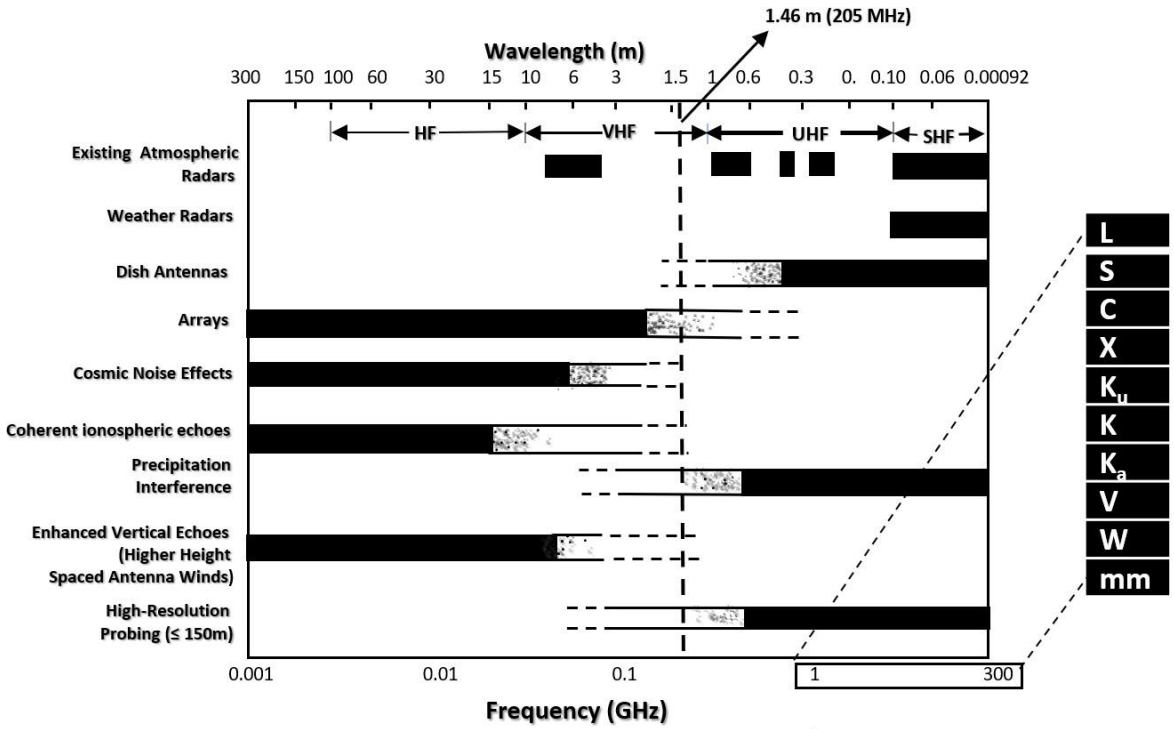

Figure 1: Graphical representation of the factors influencing the choice of frequency for WPR (Balsley and Gage 1982) Courtesy: American Meteorological Society.

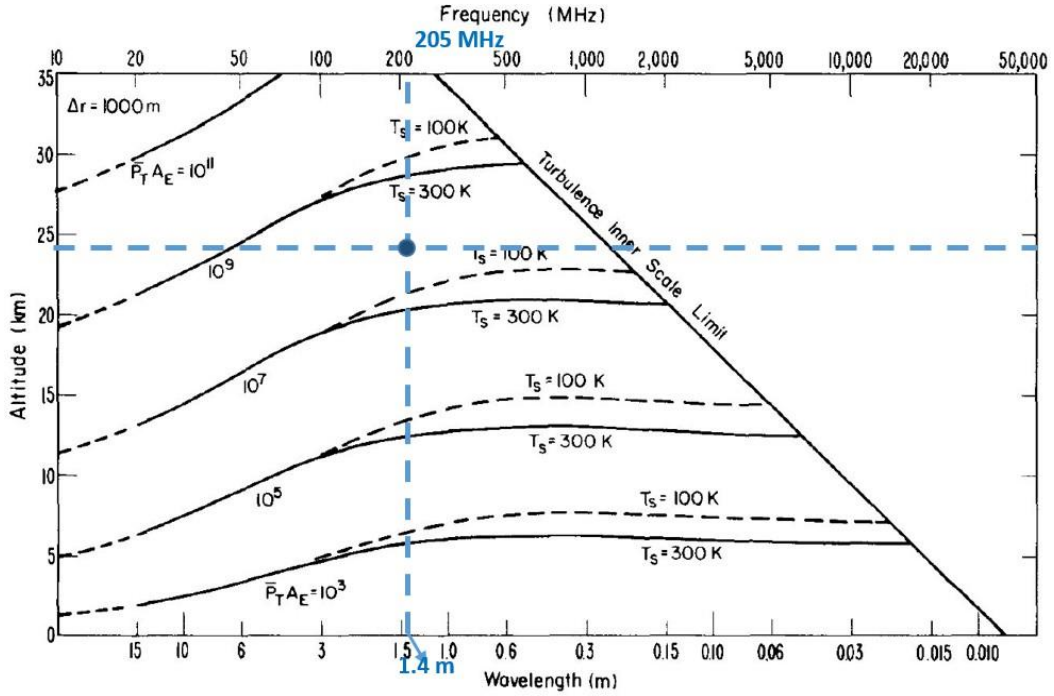

Figure 2: Maximum observational altitude as a function of frequency and power aperture product (Balsley and Gage, 1982).

as illustrated by Balsley and Gauge [5]. Because of the quick decrease in cosmic noise with frequency, the maximum visible height in the VHF frequency band increases. For frequencies beyond 100 MHz, the contribution of cosmic noise is so negligible that an increase in observed altitude can be accomplished by reducing system noise. The 200 MHz radars can achieve height coverage of 20 km by keeping the PAP of 108 Wm2.

Wind profiling radar, which operates in the 50 MHz cannot detect winds below 2 km altitude since large

aperture array cannot form a well-defined beam in the first few kilometres above the surface. WPRs operating in the UHF band (300-1200 MHz) have no data coverage in the high troposphere or lower stratosphere. However, in all seasons, the ST radar in the 200 MHz frequency band can probe the atmosphere from 315 m to 20 km. As a result, it is a compromise between the 50 MHz and 400 MHz bands and offers a once-in-a-lifetime chance to investigate atmospheric dynamics and stratosphere troposphere interaction processes in the upper troposphere lower stratosphere region [8]. Wind data vertical resolution is coarser (150 m) for the 50 MHz bands compared to the 200 MHz range (45 m). Another advantage of the 200 MHz band is that it is less susceptible to galactic or cosmic noise (1000 K), whereas the 50 MHz range is more susceptible (6000 K) [9]. For wind measurements, the galactic noise is reduced and the signal-to-noise ratio is improved. A bigger physical dimension and space (100 m x 100 m) is needed for the 50 MHz antenna array. In comparison, the modest and small 200 MHz hardware uses less room (circular area of 27 m diameter) and so is less expensive. WPRs in the UHF range are known to get contaminated in rainy weather, whereas radars in the 200 MHz band are not affected by such concerns. The 200 MHz band has a distinct benefit over other brands in that there is a distinct difference between background wind echo and echo caused by falling hydrometeors.

1.2 205 MHz ST Radar at Cochin University of Science and Technology

Considering the uncertainty of using less commonly employed frequencies for atmospheric radars, as well as considering the anticipated benefits of the VHF frequency, scientists from Advanced Centre for Atmospheric Radar research, Cochin University of Science and Technology in 2011, with funding support from DST, proposed the world's first wind profiler operating at a frequency of 205MHz VHF. Preliminary tests and demonstrations were conducted using a pilot array comprising 49 elements. Subsequently, the array further developed this array into an active phased array radar with 619 elements arranged in a triangular grid, with a Power Aperture Product of 1.6 x 108 Wm2.

The circular array has a diameter of 27m and provides a coverage active aperture area of 562 m2. This radar continuously measures zonal, meridional, and vertical winds from 315 m at lower altitudes to 20 km and above, with very high resolution in both time and vertical levels, 24 hours a day. In any weather situations, this radar can continuously scan the atmosphere. This distinct frequency band has an advantage over generally used frequency bands in radars. It is also very cost-effective and requires less human involvement. Fig 3 shows the Aerial View of CUSAT ST Radar.

Figure 3: Aerial View of CUSAT ST Radar

1.3 Geographical Importance of Cochin ST radar

Cochin's unique monsoon climate, vulnerability to climate change, rich biodiversity, tourism potential, agricultural productivity, and coastal and marine environments contribute to its climatic significance. Cochin is situated on the coast of the Arabian Sea at coordinates 10.04°N and 76.33°E in the southwest region of the Indian Peninsula. The region surrounding Cochin is often referred to as the "Gateway of the Summer Monsoon" in India. This monsoon, known as the "Southwest Monsoon," arrives in the Kerala region before spreading across the rest of the country in late May or early June, bringing moisture and rainfall. The Western Ghats Mountain range lies just 100 km to the east in the same latitude belt of Cochin located parallel to the coast of Kerala, acts as a barrier, forcing the moist winds to rise and release rainfall. This results in heavy rain in these regions. The rainfall associated with the summer monsoon is crucial for agriculture, replenishing water reservoirs, and supporting the region's overall economy. The arrival of the monsoon brings relief from the pre-monsoon heat

and kick-starts the agricultural season. The coastal location of Cochin and its proximity to the Arabian Sea contribute to its vulnerability to climate change impacts, such as sea-level rise and increased storm intensity. From the Kerala coast, the monsoon gradually propagates northward, covering the entire Indian subcontinent by July. This progression of the monsoon is a critical climatic phenomenon that significantly influences agriculture, water resources, and climate patterns across the region. Keeping this geographical importance in mind, a group of researchers from Cochin University of Science and Technology have established a stratosphere-troposphere (ST) wind profiling radar operating at 205MHz in Cochin. The primary objective of this radar is to investigate the dynamics of the summer monsoon.

2. Detailed Block diagram and Technical Specifications

The CUSAT Stratosphere-Troposphere radar is a pulse-Doppler radar capable of monitoring the backscattered data to determine the Doppler shift at various heights. The system is made up of 619 Yagi Uda antennas grouped in a 27-meter-diameter circular aperture. The radar's power aperture product is constructed in such a way that the feeble backscattered signal from 20 km altitude should fall considerably above the system's sensitivity limit. The system has two operating modes: Doppler Beam Swinging (DBS) and Spaced Antenna Mode (SAM). The basic block diagram of ST Radar is shown in Figure 4. The radar system has five main subsystems: the antenna, the transmit/receive module (TRM), the distribution network, the radar computer, and the radar console. This radar system, renowned for its sophisticated design and capabilities, utilizes 619 individual elements to accurately measure and analyze wind patterns. In addition to the detailed block diagram, Table 1 presents a specification overview of the wind profiler. The ST radar installed at CUSAT is an active phased-array radar consisting of 619 three-element Yagi–Uda antennas arranged in an equilateral triangular grid with an inter element spacing of 0.7λ, where λ is the operating wavelength, which is 1.43 m. The gain of each antenna is 7.5 dBi with a voltage standing wave ratio (VSWR) of 1.2:1. The power aperture product is 1.6 × 108 Wm2 with an approximate one-way half-power beam width of 3.2°. The peak and the

Table 1. CUSAT ST Radar System Specifications

Parameters	Specifications
Frequency	205 MHz
Bandwidth	5 MHz
Type of system	Active Phased Array
Antenna element	Three Element Yagi-Uda
Height coverage	315 m to 20 km
Range gates	1024 (Programmable)
Modes	DBS/SAM
Height resolution	~ 45 m to 720m
Beam width	~ 3º
Off Zenith Angle	0° to 30° in steps of 1°
Beam positions in Azimuth	0° - 360° with 1° resolution
Pulse width	0.3 µs to 76.8 µs
Modulation	Binary Phase Shift Keying (BPSK)
Code	Complementary Code/ Barker Code
Baud rate	0.3 µs to 4.8 µs in steps of 0.3
PRF	100 Hz to 16 kHz Selectable
Peak Power	500 W (typical per element)
Duty ratio	Up to 15 % (Max)
Peak power aperture product	~ 1.6 x 10^8 (typical) Wm^2
Radar system sensitivity	-165 dBm (post processing)
Dynamic range	70 dB (min)
Master Reference Oscillator	Rubidium oscillator with short term sta- bility of 1.4E-11
ADC	16 - bit
Type of receiver	Direct band with sampling
Type of signal processor	FFT based frequency domain
Horizontal wind Velocity	Up to 70 ms^{-1}
Vertical wind velocity	Up to 30 ms^{-1}
Radial velocity resolution	Better than 0.1 ms^{-1}

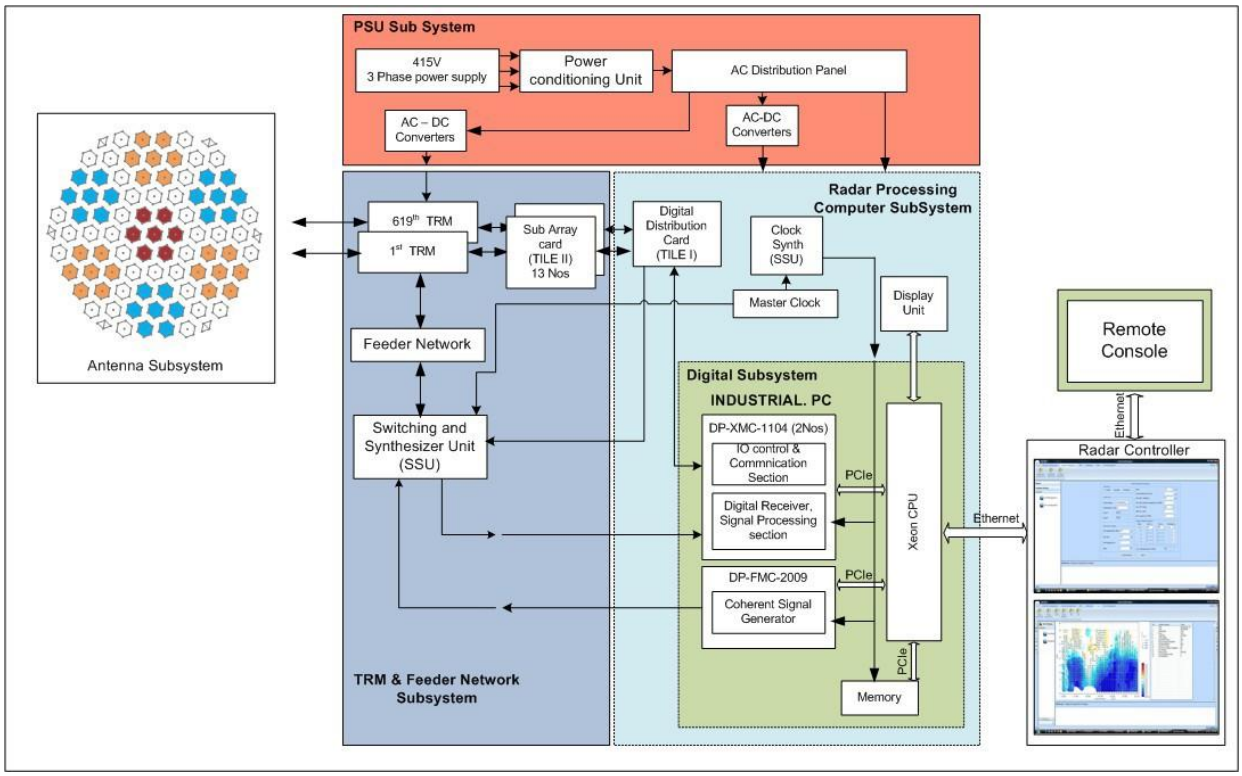

Figure 4: CUSAT ST Radar Block diagram.

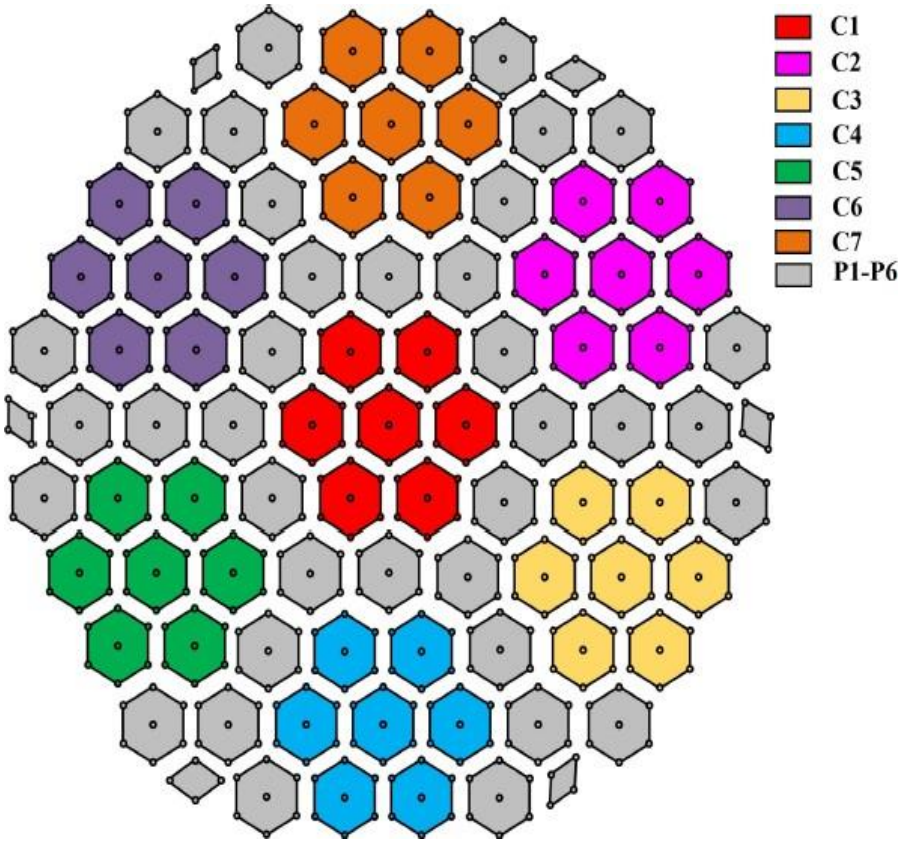

Figure 5: Cluster wise arrangement of 619 element array.

mean power of the radar are 309 and 46 kW, respectively.

The radar has a beam-steering range of 0º to 30º along elevation and 0º to 360º along azimuth, with a step of one. A three-dimensional image of the atmosphere would be possible with a resolution of 1 in both azimuth and off-zenith. The detection of backscattered electromagnetic waves induced by refractive index disturbances caused by atmospheric turbulence is the primary mechanism. Backscattered radar echoes modified by the wind at that point result from Bragg scattering caused by refractive index disturbances.

2.1. Antenna Array

Stratosphere Troposphere wind profiler at CUSAT is a phased array radar using Yagi-Uda antennae. Array is divided into 13 clusters with 7 clusters of 49 elements each and six clusters in the periphery with 46 elements each as shown in the Figure 5. Each cluster is grouped again into seven clusters of seven elements each. To avoid grating lobes all elements are separated by 0.7 λ. The effective aperture area calculated is as 536 m2 with HPBW of 3.2° and first side lobe level of -18 dB. ST radar antenna array cluster wise arrangement is shown in figure 5. The main parameter for designing an array is the half power beam width (HPBW), maximum tilt angle and power aperture product (PAP). The HPBW should be approximately 3◦, the array should be capable for tilting up to 30◦ off-zenith without any grating lobes and the power aperture product should be capable of detecting weak signals from 20 km.

2.1.1. Inter Element Spacing

In a phased array system inter element spacing is the important parameter to avoid the grating lobes. If the spacing between elements are equal to or greater than λ/2, then there will be more than one main lobe with magnitude almost same as main lobe. This is not desirable in a wind profiler system. To avoid grating lobes, the system should satisfy equation below [15]:

$$\frac{D}{\lambda} \leq \frac{1}{1 + sin\theta}$$

Where D is inter-element spacing, λ is the wavelength and θ is maximum tilt angle with respect to zenith. Inter element spacing is calculated and approximated as 0.7λ.

2.1.2. Number of elements in the array

The number of elements of an array is directly related to the half power beam width (HPBW). The empirical formulae for HPBW [15] are given by equation:

$$HPBW = 58.92\frac{\lambda}{L}$$

Where λ is the wavelength L is the aperture diameter of array. To get an HPBW of approximately 3 L is calculated as 27 meters, with an inter element spacing of 0.7λ. Approximately 619 elements are required to fill a circular aperture of 27 m diameter.

2.1.3. Gain of Array

Gain of the array depends of the individual element gain and the total no of elements. The simulation results of single 3-element Yagi-Uda antenna shows that the gain could vary from 6.5 dBi to 9 dBi. For the calculation purpose we approximate the individual gain as 7.5 dBi.

Array Gain(G) = Gain of antenna(dBi) + 10 log(N)
Where N is the no. of Yagi antennas in the array.
Array Gain(G) = 7.5dBi + 10 log (619) = 35dBi

2.1.4. Effective Aperture Area

Effective aperture area (Ae) determines how effective an antenna can transmit or receive electromagnetic radiation. It can be computed as.

$$A_e = \frac{\lambda^2 G}{4\pi}$$

Where G is the array gain, and λ is the wavelength at operating frequency. In the case of 205 MHz radar, λ is 1.463 m. The effective aperture area thus becomes 538 m2. The array gain(G) depends on the individual element gain and the total number of elements [15]. The simulated gain of the Yagi-Uda antenna is 7.5dBi.

2.2. Transmit Receive Module (TRM)

The fundamental advantage of a phased array system is that the main lobe may be electronically

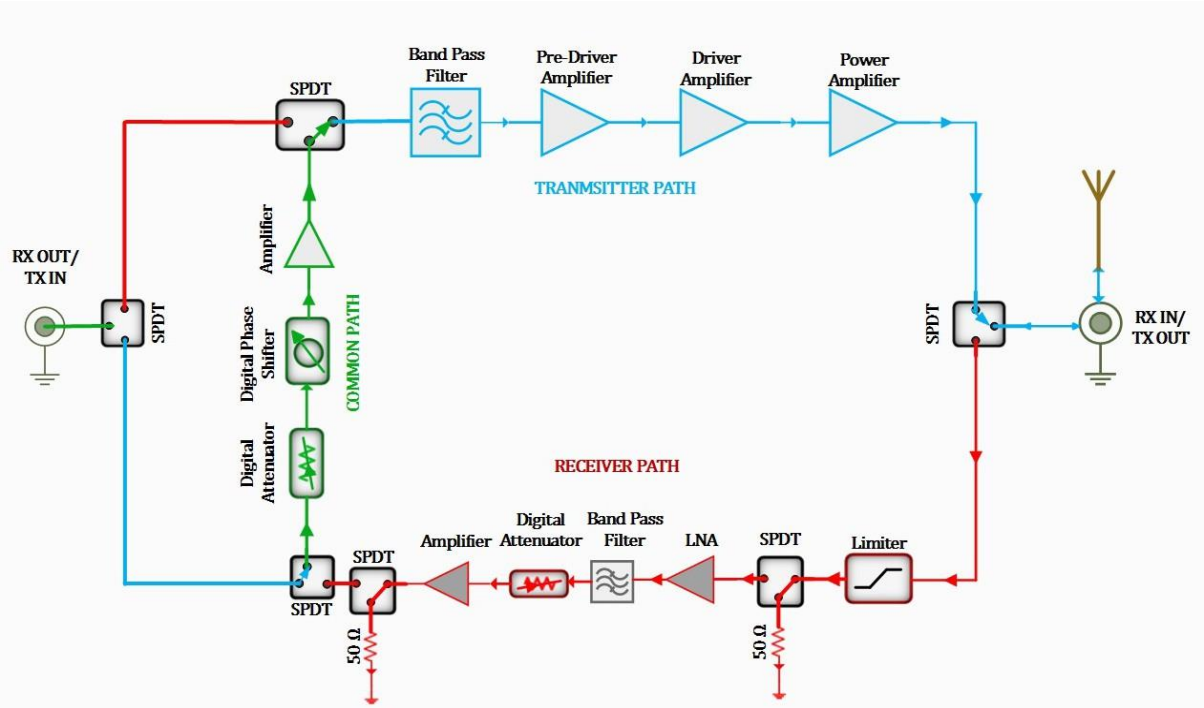

Figure 6: ST Radar transmits receive module block diagram.

steered in any direction without any mechanical antenna tilting. This will also lower maintenance costs due to mechanical wear and tear. Beam scan and beam-to-beam changeover times can both be lowered. All of this is feasible due to the advancement of individual TRM in the phased array system [13]. The TRM and feeder network serve as a link between the antenna and the radar processing computer. In transmission, the DAC generates an RF signal that is dispersed to the 619-element antenna array. All signals are merged and connected to the ADC when in receiving mode.

TRM is composed of up of four sections: a high-power transmitter portion, a low power reception section, a power supply card, and a digital section. The TRM, in conjunction with the power amplifier, provides the needed gain and phase for the transmitter and received RF signal. The block diagram of a TRM is shown in Figure 6.

The main functionalities of TRM are;

(i) Depending on the TR pulse from radar processing computer, the TRM activates the transmit path or receive path.

(ii) During the transmit cycle, TRM will give an amplification of 57 dBm to the input RF signal.

(iii) Along with the LNA in the receive chain will boost the by 42 dB.

(iv) Will provide appropriate progressive phase shift for electronic beam steering using 6-bit phase shifter during the Tx and Rx modes.

(v) The limiter in the Rx section will protect the low power Rx section from the high power leakage from the Tx section during transmission.

TRM's transmit chain is made up of a series of amplifiers, band pass filters, and phase shifters. The phase shifter shared by the Tx and Rx paths will provide the appropriate phase shift to the input RF signal for beam steering. The transmit chain provides a 500 W peak power RF signal with a bandwidth of 5 MHz at 205 MHz. Amplification of 57 dBm output power is provided by the pre-driver amplifier, driver amplifier, and power amplifier. A band pass filter with a bandwidth of 5 MHz is used to limit the operational bandwidth. The TRM operates in pulse mode, with a duty cycle of up to 15%. To assess TRM effectiveness, the output power, rise time, fall time, and harmonic measurement are necessary.

The receiver module will amplify the RF signal which is backscattered from atmosphere. The Rx path is designed to operate at 205 MHz with an

operational gain of 40 ± 2 dBm and a noise figure of less than 3.5 dB. High power Tx path and low power Rx path is connected to the same antenna through a T/R switch. There is a possibility of leakage of Tx pulse into Rx path. To protect the low power Rx path a limiter diode is provided at the front end just after the T/R switch connected to antenna. One more T/R switch is placed between limiter and LNA to prevent LNA going into saturation mode. Band pass filter is connected to limiter so that the bandwidth of operation can be limited to 5 MHz. An attenuator is placed for gain tapering application. Table 2 shows the specification of Rx path components.

Table 2. CUSAT ST Radar TRM specifications.

Parameters	Specifications
Frequency	205 MHz
Transmit input power	-10 ± 2 dBm
Output power	57 dBm
Pulse width	0.3 µs to 76.8 µs
Duty Ratio	Up to 15%
Receiver chain gain	40 ± 2 dB
Receiver noise figure	< 3.5 dB
Harmonic level at Tx	< -30 dBc
Rise time	< 100 ns
Fall time	< 100 ns
Digital attenuator	0.5 to 31.5 dB with steps of 0.5 dB
Digital phase shifter	5.625° to 354.375°
Interface	RS 422
Supply voltage	48 V DC
Supply current	6 A

2.3. Feeder Network

ST Radar employs three steps of power combiner/divider (PCD) to channel RF power to 619 TRMs in transmission and reception modes. The signal from the coherent signal generator is routed to 619 TRMs during transmission mode, and the signals received from TRMs are aggregated and routed to a digital receiver during reception mode. Signals are sent between the TRM and the Radar Processing Computer via a series of PCD. The feeder network is made up of three separate PCD phases. The first stage employs 1:13 PCD, the second employs 1:7 PCD, and the third employs 1:8 PCD, all of which are bidirectionally coupled to form the ST Radar feeder network. The first stage power input is connected to the digital receiver and coherent signal generator through a switch controlled by a TR pulse. Figure 7 shows the schematic representation of feeder network. During transmission, the network is linked to a coherent signal generator, and during reception, the network is linked to a digital receiver.

2.4. Radar Processing Computer (RPC)

The radar processing computer (RPC) is considered the heart of the system. All the control signals, RF generation and sampling modules are placed inside the RPC. It consists of a coherent signal generator, digital receiver, and control signal generator. The control signal generator produces the TR pulse, gain control, and phase programming of TR modules and monitors the health status of TRM. Coherent signal generators have the pulsed carrier signal at 205 MHz, amplified by the TR module and transmitted through the antenna array. The analogue-to-digital converter (ADC) digitises the backscattered signal with a sampling rate of 80 MHz. The signal from ADC is down converted to 10 MHz using a direct digital converter (DDC). The RPC performs all the signal processing operations, and parameters like Doppler width, mean Doppler and wind vectors are analyzed.

2.4.1. Coherent Signal Generator

The RF signal generator is field-programmable gate arrays (FPGA) based dual channel 14-bit digital to analogue converter (DAC) card. It consists of two highspeed DAC. The external clock of 840 MHz is fed from the clock synthesiser unit. The DAC receives the baud, code length, and cord word from the radar controller, and generates the RF signal based on these parameters. The DAC can generate complementary as well as barker-coded signals. The main features of DAC are (i) dual-channel DAC,

(ii) 840 MHz sampling rate, (iii) 14-bit resolution, (iv) the output power level of -3dBm, (v) spurious-free dynamic range (SFDR) -70 dBc, and (vi) 50-ohm analog output [11].

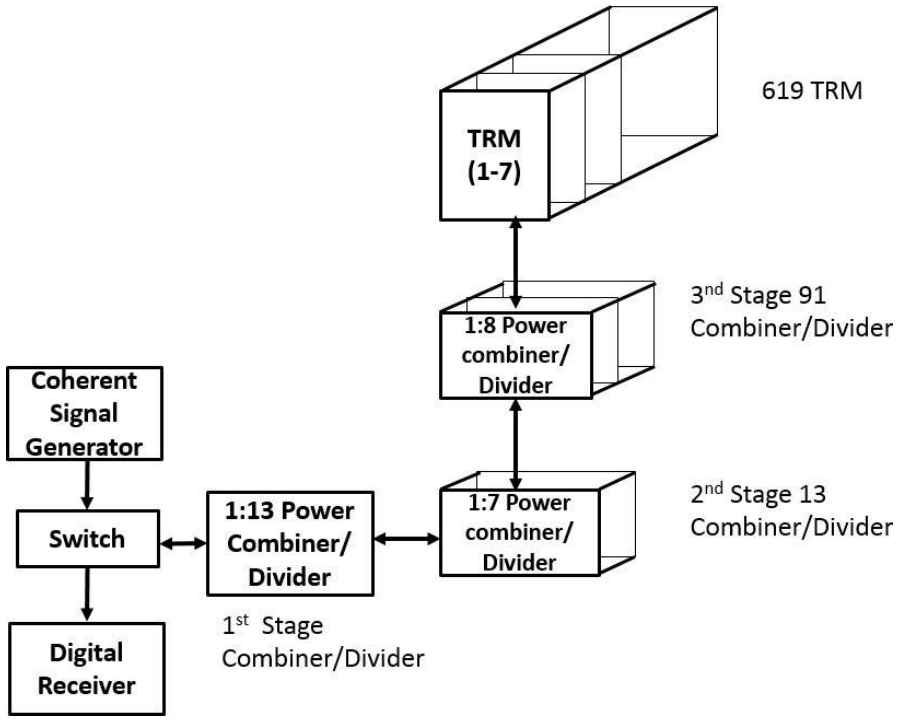

Figure 7: Schematic representation of ST Radar feeder network.

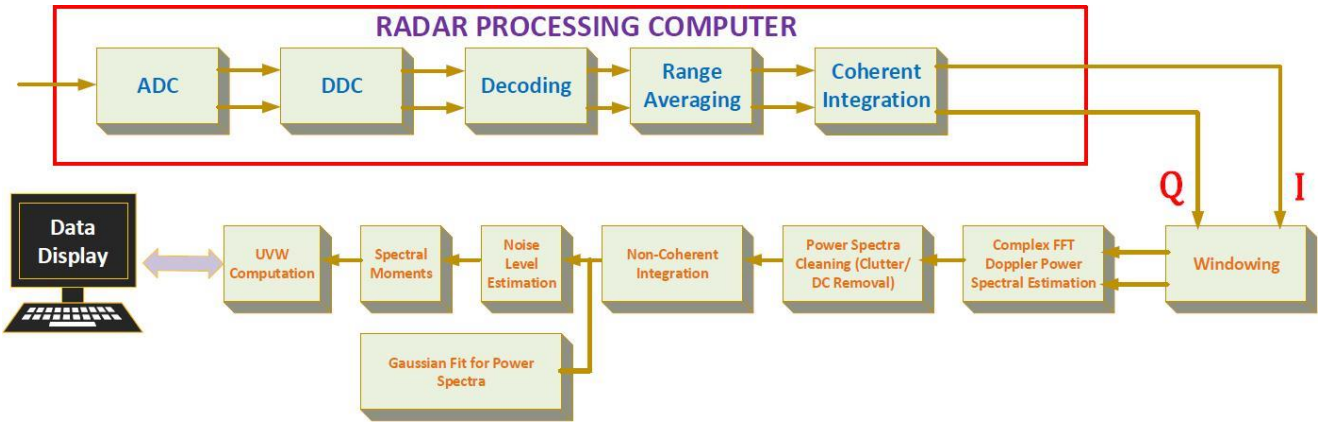

Figure 8: Block diagram of Radar signal processing.

2.4.2. Digital Receiver (ADC)

System consists of two numbers of dual channel ADC i.e. total 4 channels. Out of this 4 channel one channel is dedicated to DBS mode and other three channels are dedicated to SAM mode. The main features of ADC are (i) Two dual channel ADC (ii) 80 MHz sampling rate (iii) 16 bit ADC (iv) SFDR 85 dBc (v) SNR 74 dBc (vi) Effective number of bits is 12.3

2.4.3. Digital Signal Processing

The basic block diagram of ST Radar signal processing is shown in Figure 8. At 205 MHz, an RF signal backscattered from the atmosphere is captured using an ADC with a sampling rate of 80 MHz (under sampling). FPGA is used inside RPC to perform pulse decoding, range averaging, and coherent integration. RPC offers I Q data sample time series. Windowing is used in time series I Q data to prevent spectrum leakage. Window styles include Hanning, Hamming, Blackman, Blackman Harris, Bartlet, and Rectangular. After windowing, Fourier analysis is used to estimate the power spectrum. DC and clutter are removed in the frequency domain. Incoherent integration is accomplished by increasing the power spectrum to improve signal strength and noise reduction. The power spectrum is used to evaluate the moments reflected power (M0), mean Doppler (M1), Doppler

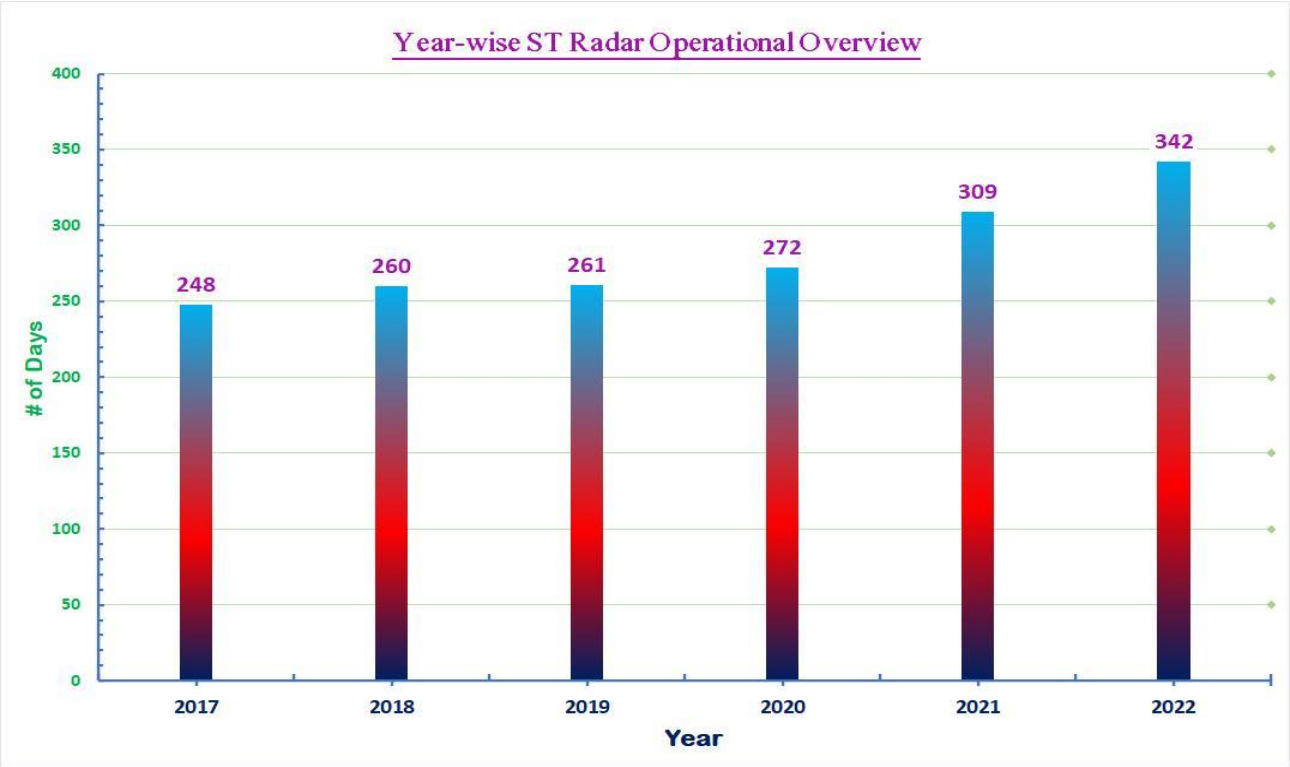

Figure 9: 205 MHz ST radar operational days for past.

width (M2), SNR (M3), and noise level (M4). These five moments are the fundamental derived parameters from the atmosphere. The wind parameters Zonal (U), Meridional (V), and Vertical (W) are calculated and shown based on the moments.

2.5. Radar Console

The ST Radar console is a Windows PC-based device that connects to Linux systems. It works as a radar control centre, giving a user-friendly interface for administering and monitoring radar functions. The Windows console software connects to the Linux system, allowing smooth integration and communication between the two platforms. This configuration allows radar operators to take advantage of the advantages of the Windows environment, such as intuitive graphical interfaces and wide programme compatibility, while also utilising the power and reliability of Linux for radar processing and data analysis. The ST Radar console combines the benefits of both operating systems to effectively enhance radar operations.

3. Radar operational Statistics

ST radar operates on a regular basis, taking normal wind data in Doppler Beam Swinging mode from 315 m to 20 km. The radar is currently operational for 15 hours on average and taking nearly three synoptic hour observations (11:30 AM, 05:30 PM, and 11:30 PM IST). Radar data is processed and preserved on a daily/weekly basis in the centre's Network Attached Storage, and the data is available for research students at all levels L0, L1, and L2. The radar control room keeps an operating log that includes the time of operation, weather conditions, and maintenance activity. Figure 9: 205 MHz ST radar operational days for past 6 years.

Wind profiling radars over the tropical region with height coverage beyond the tropopause pose obstacles in frequency selection and system-level performance parameter optimisation, such as the power aperture product. The primary reason is that the tropical tropopause is located between 16 and 18 km above sea level. The 205 MHz radar in Cochin's near-equatorial zone is chosen to explore troposphere stratospheric exchange mechanisms. Because the scale size of irregularities causing Bragg scatter is a direct function of height, this frequency band needs a considerably larger PAP to satisfy the SNR required for estimate accuracies.

In the regular and monsoon modes, there are three different configurations with height coverage of 0.3

Table 3. Comparison of existing wind profilers.

Frequency of Operation	**53 MHz**	**205 MHz [8] [18]**	**449 MHz**	**915 MHz**	**1280 MHz**
Antenna Type	Yagi -Uda	Yagi - Uda	Coaxial Collinear	Microstrip Patch	Microstrip Patch
Antenna Diameter	110 m	27 m	6 m	2 m	2.8 m
Half Power Beam Width (HPBW)	3°	3°	10°	10°	5°
Peak Power	2.5 MW	0.309 MW	2 kW	0.5 kW	1.2 kW
Height Coverage	1 – 25 km	0.315 – 20 km	0.18 – 10 km	0.12 – 4 km	0.1 – 4 km

to 8 km, 3.1 to 20 km, and 6 to 32 km. To determine the seasonal variation of higher height coverage, radar measurements from 6 to 32 km are plotted in time series. Figure 10 depicts a time series plot for 2018; the height coverage was greater than 19 km in all seasons in 2018.

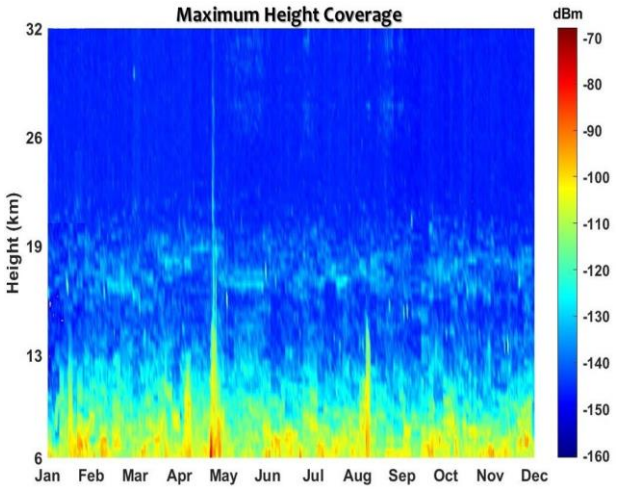

Figure 10: height coverage of 205 MHz ST radar for an entire year.

3.1 Comparison of 205 MHz ST Radar with existing wind profiler radars

Well established wind profiler radars are centered around 50 MHz, 449 MHz, 915 MHz and 1280 MHz. Table 3 shows the comparison of different existing WPR. The comparison shows that to cover an altitude of 300 m to 20 km with less input power and small aperture area, 205 MHz is the best choice.

4. Validation of radar wind data with GPS radiosonde measurements

Winds measured by a co-located GPS-based radiosonde (GRAW radiosonde) are commonly used to evaluate and compare radar-detected winds. The GRAW radiosonde measures wind speed (0.1 ms-1) and direction with finer vertical precision (4 to 5 m) than other radiosondes. The radar was tested using three different coded modes with baud rates of 0.3, 1.2, and 2.4 s, and the results were compared to radiosonde readings. Figure 11 shows a comparison of wind components measured on December 13, 2016. The zonal (u) and meridional (v) wind components from radar data correlate reasonably well with the radiosonde component [17].

Furthermore, wind speed corresponds more closely at lower elevations than at higher levels. The difference at higher altitudes could be attributed to significant horizontal drifts of the balloon from the launching point over time because of the prevailing wind. During the one-year validation period, the correlation for the zonal component is 0.99 and for the meridional component is 0.96. The radar system is meant to recover wind speed with a 1 ms-1 accuracy for horizontal components and 0.1 ms-1 accuracy for vertical components. In general, radar wind profiles correlate quite well with radiosonde wind observations for altitudes ranging from 315 m to 20 km [17][18].

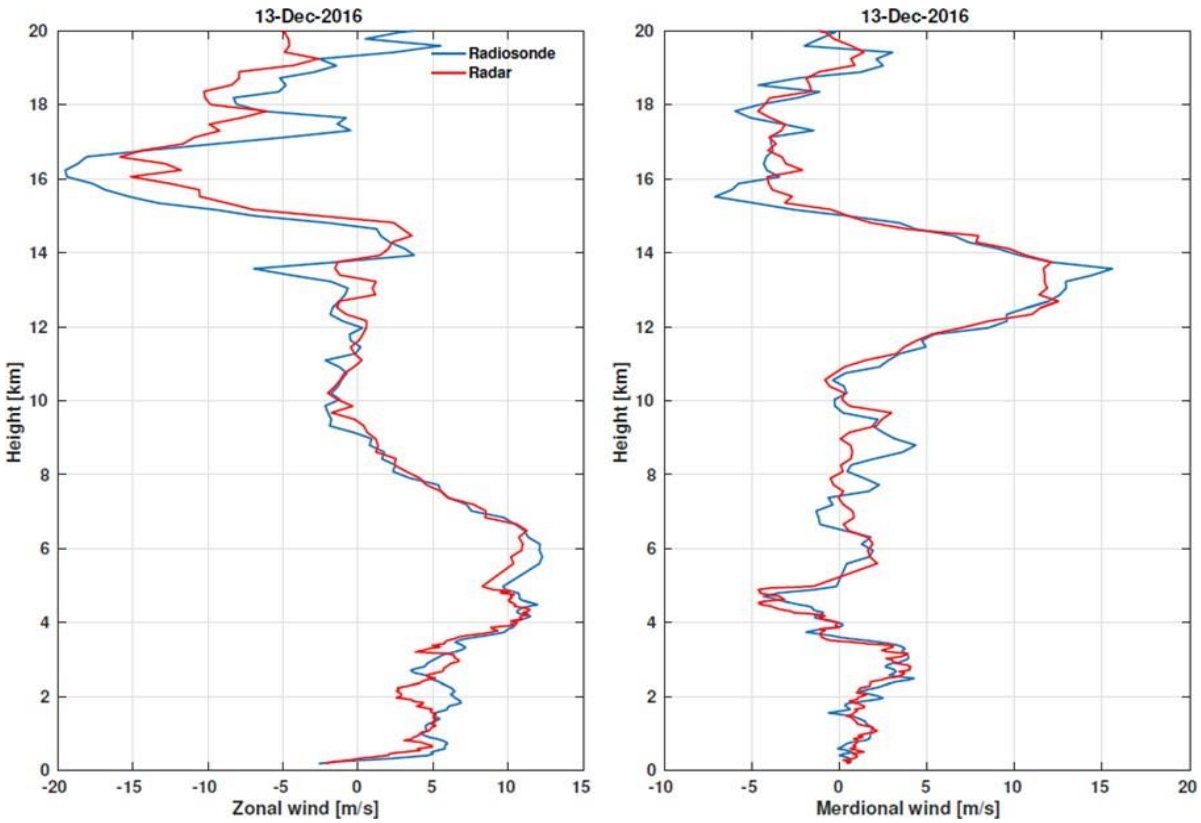

Figure 11: Wind derived from radar (u and v components on the left and right, respectively) versus radiosonde (Mohanakumar et al.,2018).

4.1 Validation methodology

GRAW DFM-09 radiosonde is used to validate the performance of the ST radar. The DFM-09 includes a code-correlated GPS receiver. The GPS position data is sent to the ground station and is adjusted with the ground station. These corrected data are used to determine the wind speed and direction correctly at all heights. The radiosonde ascent will cover up to 25 km from the ground station on average, with a vertical resolution of 25 m. The radiosonde's drift with the wind flow allows for the calculation of horizontal wind speed and direction. The manufacturer's predicted accuracy of the wind speed is < 0.2 ms-1.

To validate the radar wind profiles, we ensured that radiosonde wind measurements were matched with radar data both in terms of location and time. Radar profiles were created every 3 minutes, while radiosondes provided data every 5 seconds. These matching instances with radiosondes were determined based on the timing of radar data acquisition. For each instance of radar data collection, we made sure to pair it with corresponding radiosonde data. Consequently, there were situations where we had pairs of data that were closely aligned in both location and time. The collocated pairings with an average altitude difference of 25 m and the greatest temporal difference of 300 s were kept. The zonal (u) and meridional wind (v) components were computed from the collocated radiosonde wind speed and direction and then compared to the radar's zonal and meridional winds for the altitude range of 0. 3-20 km. Collocation criteria ignore radiosonde drift during ascent, instead focusing on differences in vertical height and data acquisition time [17].

Some exclusions were applied based on wind speed and direction parameters before directly comparing radiosonde and radar data. Data points with wind direction offsets greater than 90 degrees or mild winds less than 2 m/s with significant speed variances were eliminated. To achieve rigorous comparisons, data points with a wind speed difference greater than 7 m/s were eliminated. These exclusions are intended to improve data quality. It is crucial to remember that considerable wind speed disparities can arise if radiosondes drift

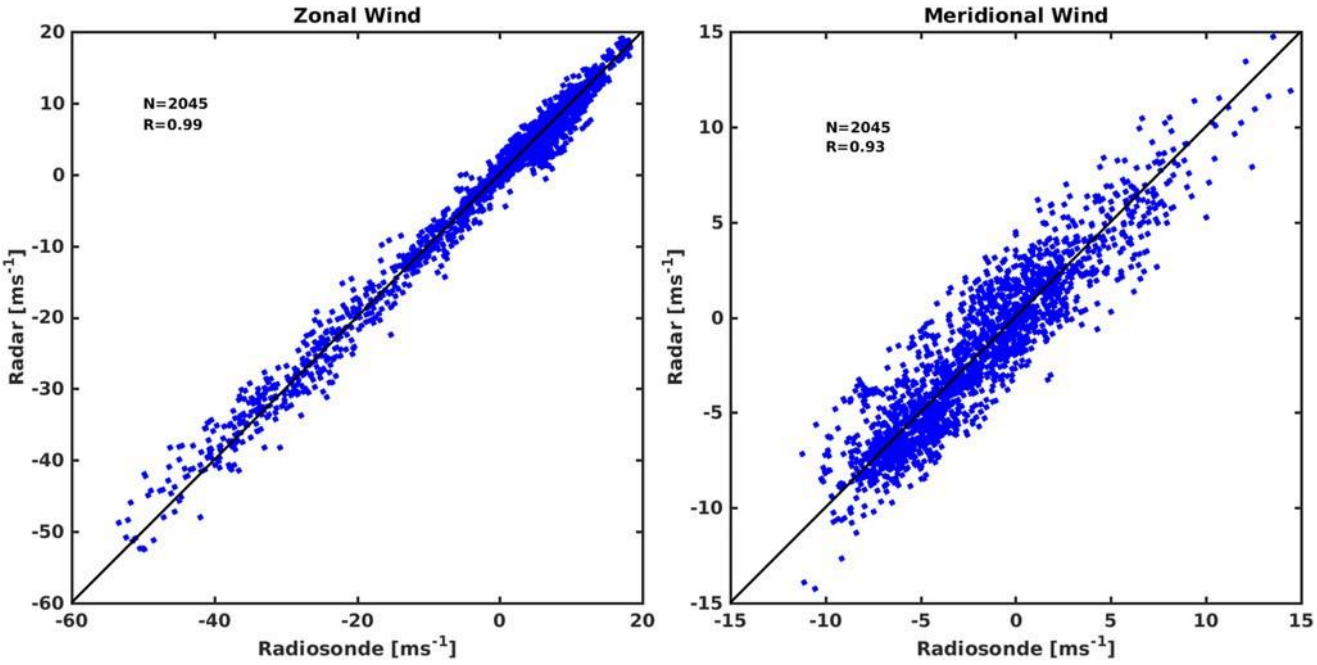

Figure 12: Scatterplots of radar vs radiosonde zonal and meridional winds. The case where the abscissa and ordinate are identical [i.e., it has a slope of unity and passes through (0, 0); black line] is indicated. (Mohanakumar et al.,2018) [18].

too far away from the radar position, but this does not necessarily imply inferior comparisons. Local changes in temperature or pressure fields caused by turbulence can also contribute to such variations.

4.2 Radar Versus Radiosonde Comparison

Figure 11 depicts the wind speed and direction patterns observed by radiosonde and radar on August 22, 2016. The radar gave a traceable signal from 315 m to around 22 km on that day, and the comparison indicates that the radar-derived wind speed and direction correlate well with the radiosonde profiles. Overall, the results reveal that the radar can provide very precise wind profiles for altitudes ranging from 315 m to 20 km.

Scatterplots in figure 12, depict the comparison between collocated radiosonde and radar zonal and meridional winds spanning altitudes from 315 m to 20 km. These collocations are based on spatial and temporal constraints, considering that radar profiles are generated every 3 minutes. The collocated pairs are determined by selecting the closest height and time between the radar and radiosonde measurements, with maximum differences of 18 minutes in time and 32 meters in height. For further information on collocation techniques, refer to Kottayil et al. (2016) [17].

The radar's horizontal wind components exhibit remarkable agreement with radiosonde data, displaying a mean bias of 0.053 ± 1.85 m/s in zonal wind and 0.005 ± 1.66 m/s in meridional wind. Pearson correlation coefficients between radar and radiosonde measurements are 0.99 for zonal wind and 0.93 for meridional wind, both significant at the 0.01 level. Linear regression slopes are 0.97 for zonal wind and 0.93 for meridional wind. It's important to note that this comparison assumes zero error in radiosonde data, though a more comprehensive comparison considering errors in both radiosonde and profiler winds is discussed in Kottayil et al. (2016) [17].

4.3 Rain signature in Radar spectra

VHF radars are known to be sensitive to Rayleigh scattering during precipitation (Fukao et al. 1985) [39], which can be used to retrieve microphysical features of precipitating clouds such as raindrop size distributions (RDSDs) and the fall speed of a precipitation particle, among other things. Figure 8 depicts the Doppler power spectrum on a rainy day. The image clearly shows two separate power spectra: one centred around 0 Doppler represents ambient air echoes, while the other located about 8 ms-1 reflects precipitation echoes. Martin Ralph (1995) [40] defined the observed Doppler power

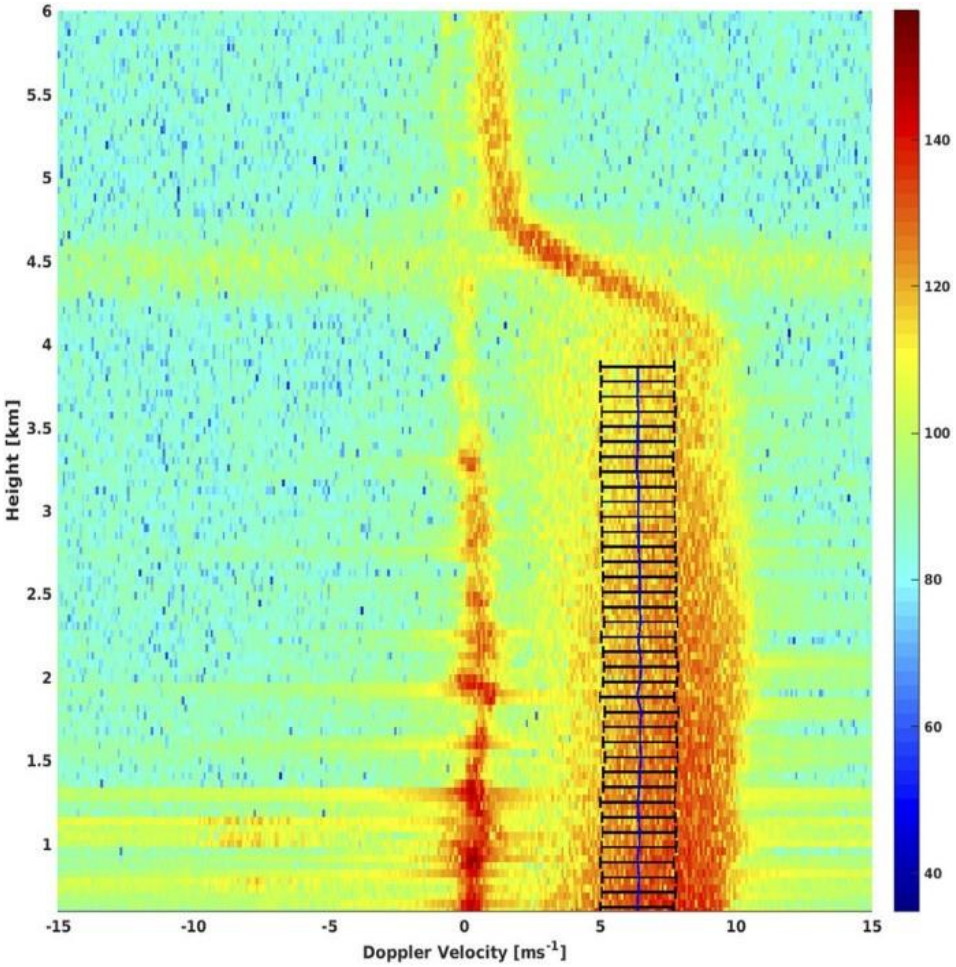

Figure 13: The Doppler power spectrum of the zenith beam observed during the rainy day of 18 May 2017. The power (dB) is uncalibrated. The mean Doppler (blue) and the Doppler width for rain echoes (black) are indicated. (Mohanakumar et al.,2018) [18].

spectrum at 8 ms-1 as the convolution of Bragg scattering from ambient air and Rayleigh scattering from precipitation. Elimination of air vertical motion from the precipitation-affected Doppler power spectrum is the most critical step in obtaining RDSD or raindrop fall velocity from VHF radar readings. After deconvolution, the RDSD and fall speed can be calculated using numerous methods.

As seen in figure 13, the 205-MHz ST radar readings clearly separate the ambient air portion from the precipitation portion. Furthermore, the presence of a melting layer as a horizontal strip is plainly seen in the power spectra at approximately 4.5 kilometres. This demonstrates the radar's capacity to distinguish between different levels of rain-bearing clouds.

Dhanya et. al. (2022) [42] discusses a novel hybrid approach applied to a 205-MHz ST radar for distinguishing between clear air and rain echoes. Conventional techniques struggle to differentiate the two echoes due to merging during rainy periods. The hybrid approach uses an adaptive fitting algorithm with a bi-Gaussian model to identify distinct peaks. The number of peaks is confirmed through zero-crossings of the power gradient. The method has been tested on various weather conditions and shows promising results. The approach allows for accurate separation of clear air and precipitation echoes, providing new avenues for ST radar signal processing. The adaptive algorithms, such as the Least Mean Square (LMS) and Normalized Least Mean Square (NLMS), are applied in Dhanya et. al. (2021) [41] to separate clear air echoes from precipitation echoes. The NLMS algorithm performs better in distinguishing between the two types of echoes, especially during heavy rain conditions. The results show that the adaptive algorithms improve the accuracy of wind

velocity computation and enable the identification and separation of clear air and precipitation echoes.

5. Scientific Applications of 205 MHz ST Radar at CUSAT

MST/ST radars are now well recognised in the radar meteorology field as an important supplement to weather radar measuring techniques that rely on Rayleigh scattering from hydrometeors. These radars detect echoes induced by Bragg scatter from refractive index structure owing to humidity and temperature fluctuations in both clear and overcast atmospheric circumstances. Some of the intriguing studies from the 205 MHz ST radar observations from a tropical coastal station in Cochin are reported in this section.

The Indian summer monsoon (ISM) is a widely debated annual occurrence. The arrival of the monsoon causes significant changes in atmospheric circulation. It manifests itself by producing two distinct monsoon circulations, the lower troposphere's low-level monsoon jet (LLJ) and the upper troposphere's tropical easterly jet (TEJ). Changes in monsoon jet stream flow patterns during the active/break phase might influence the course and distribution of monsoon rainfall over the Indian subcontinent [19][20]. Monitoring the vertical structure of monsoon circulation is required to fully comprehend monsoon activities. Furthermore, measurements on monsoon circulation are critical for evaluating circulation properties using model simulations. The CUSAT ST radar is unique in that it is located at the beginning of the Indian summer monsoon. The radar provides remarkable insight into the evolution of monsoon circulation. Kottayil et al. [21] used radar data from April to September for two consecutive years, 2017 and 2018, to try to determine the vertical structure of the monsoon circulation. The study primarily investigates the feasibility of objectively establishing predictors of monsoon start. For the first time, wind profiler data from Cochin is used in this work to understand the start and

advancement of the Indian summer monsoon circulation. More process studies that investigate the detailed vertical structure of monsoon circulation during the onset are needed to advance our understanding of one of the most difficult processes to describe. With the introduction of 205-MHz wind profiler radar, we may be able to better monitor and understand the variables that lead to monsoon start and progression.

ST Radar capability has been explored to find the atmosphere response to the annular solar eclipse of December 2019.Along with radar, automatic weather station (AWS) and GPS radiosonde were used to record the variations in weather parameters on and pre and post-day of the solar event. The mean planetary boundary layer and tropopause height reduced by 50 % and 5.5%, respectively, were noted in the study. Another significant finding was the presence of internal gravity waves with a 40–60-minute periodicity [22].

In three consecutive winters, 2016/17, 2017/18, and 2018/19, radar observations of wind profiles in Cochin have been used to study the vertical coupling between the stratosphere and troposphere. The observations reinforce the classical features of sudden and abrupt warming manifested in the form of a reversal in horizontal upper tropospheric winds and a change in its magnitude. During the sudden stratospheric warming (SSW), upper tropospheric zonal winds decreased or reversed their prevailing direction. Sudden fluctuation in the vertical wind and abrupt fall in Outgoing Longwave Radiation (OLR) followed by convection resulting in extreme rainfall observed [23] shown in figure. 14. Wind profiler data was used to understand the monsoon low-level jet during the Kerala floods in 2018. High moisture levels due to westerlies' enhanced speed and depth worsened the condition, leading to a deluge [24].

Experiments conducted in a special mode detected echoes from the ionosphere for the first time from 205 MHz radar near the equator. Field alignment irregularities were identified in the E and F regions by the received echoes. E-layer irregularities were Type 2 in nature as shown in figure 15 [25]. E-layer disturbances between 90 and 110 km were observed during the equinox, summer, and winter. These disturbances have a varying life span from a few minutes to several hours. Morning and afternoon E-layer echoes were continuous, whereas late afternoon was quasiperiodic [26].

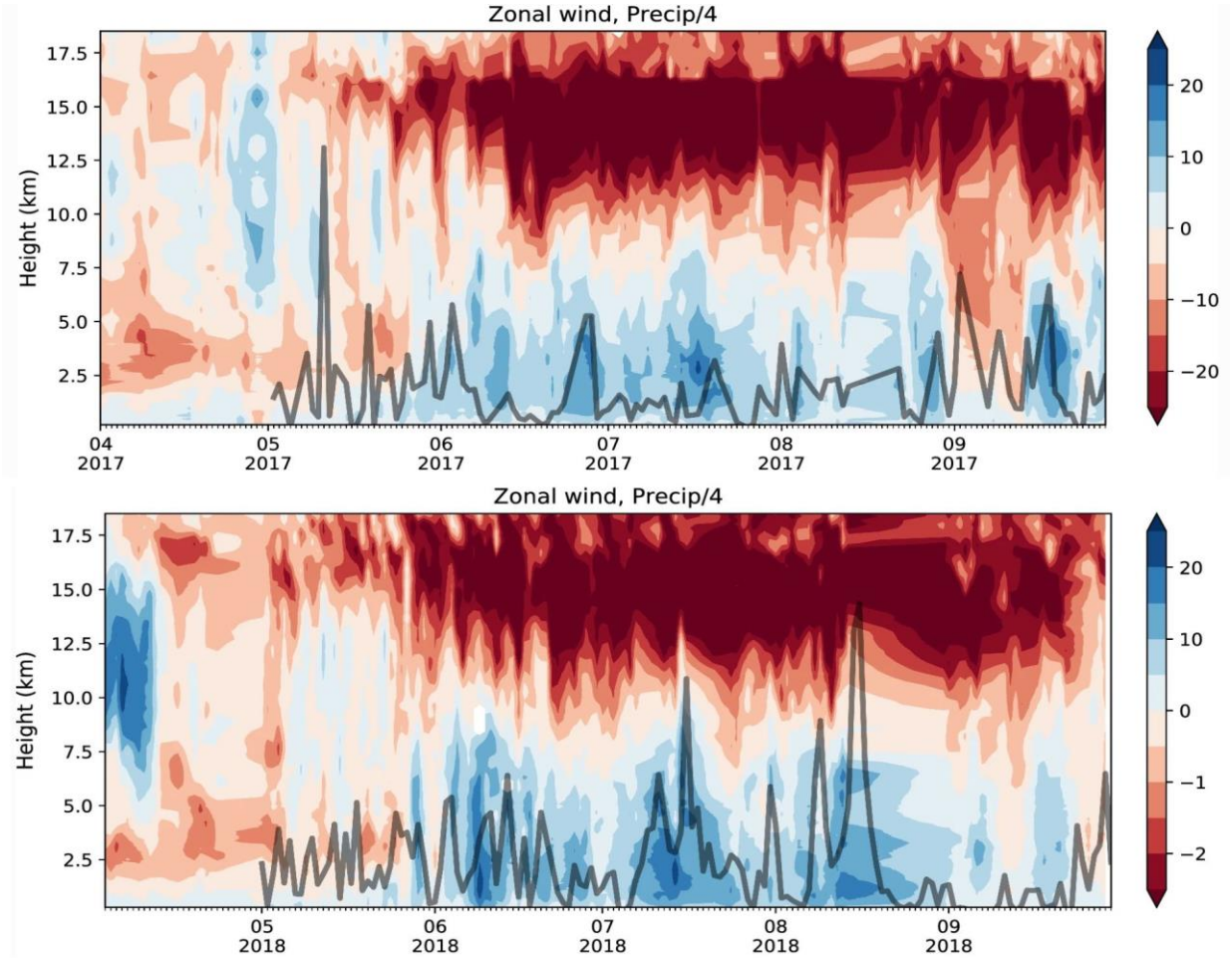

Figure 14: Distribution of zonal wind in the troposphere and lower stratosphere during the two consecutive monsoon years 2017 & 2018. The tick lines indicate the precipitation values (Kottayil et.al.,2019).

The 205 MHz ST radar at CUSAT Kochi, India, is utilised to research the ionosphere and its interactions with space weather phenomena. Here are some instances of space weather incidents that this radar can or may be able to detect:

(i) Ionospheric disturbances: Space weather phenomena such as geomagnetic storms, solar flares, and coronal mass ejections can create ionospheric irregularities, which the radar can detect and analyse. These disruptions have the potential to disrupt radio wave propagation and communication systems.

(ii) Scintillations: The radar can detect the intensity changes of radio signals induced by small-scale ionosphere anomalies. Scintillations are common during times of increasing solar activity and can have an influence on satellite communication and navigation systems.

(iii) Plasma irregularities: The radar may detect ionosphere plasma irregularities such as plasma bubbles and plasma depletions. These anomalies can interfere with radio wave transmission and degrade the functioning of satellite-based devices.

(iv) TIDs (travelling ionospheric disturbances): TIDs are wave-like disturbances that propagate in the ionosphere and can be detected by radar. TIDs can be triggered by a variety of space weather events and can have a substantial impact on radio wave propagation over long distances.

(v) Variations in Total Electron Content (TEC): TEC, or the total number of free electrons along a path through the ionosphere, can be measured using radar. Space weather events can cause TEC changes, which can have an impact on satellite-based navigation systems like GPS. Shown in figure 16.

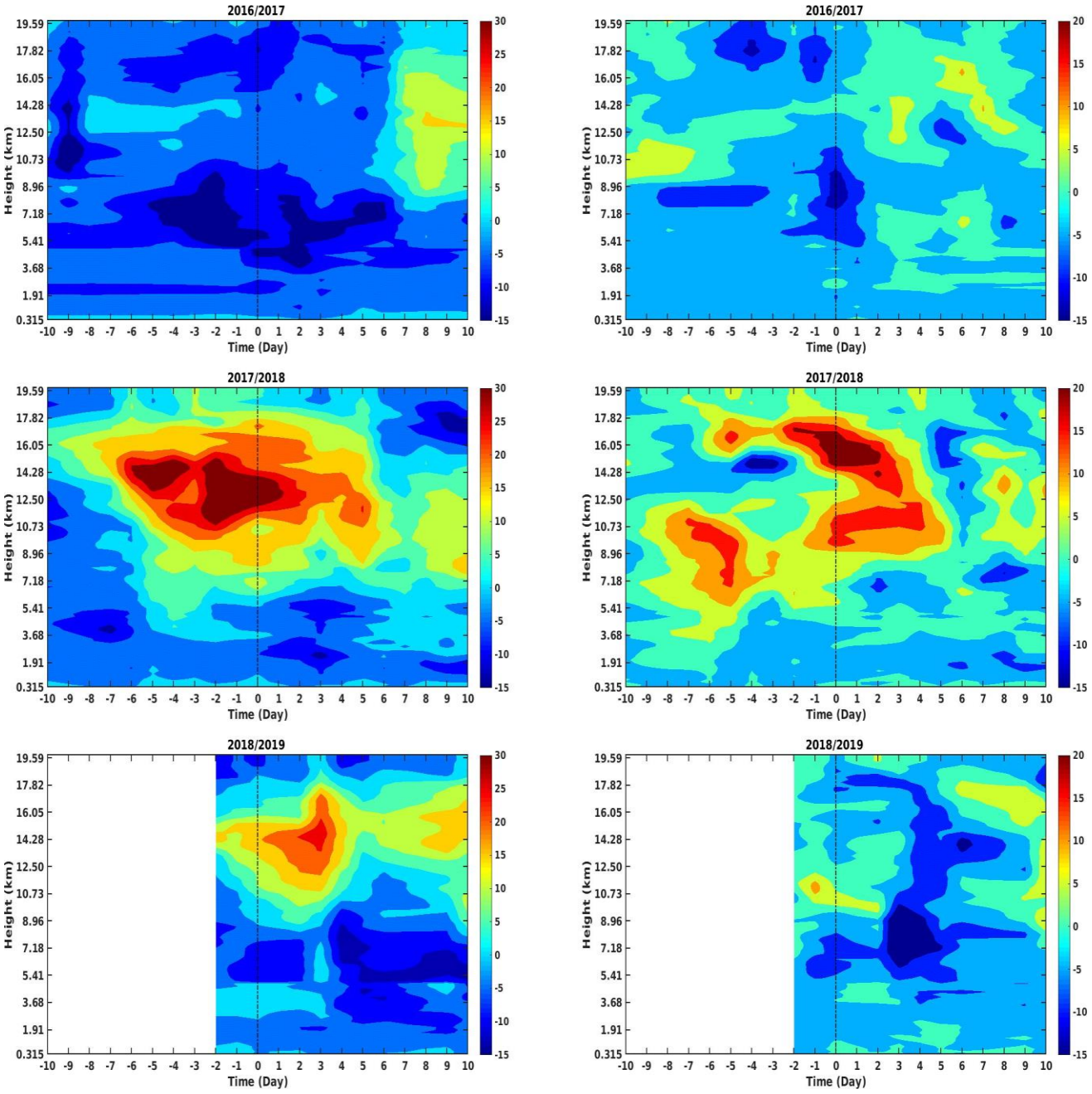

Figure 15: Height Time Intensity plot of Zonal (Left panel) and meridional winds observed from ST radar observations at Cochin during sudden stratospheric events (Remya et.al.,2021).

Submarine volcano Tonga–Hunga Haʻapai in the southern Pacific Ocean erupted in December 2021-January 2022 and was the largest of its kind in this century. The eruption generated internal gravity waves (IGW), spreading over the globe. Plume-like structure at a height range of 276- 550 km for 4.5 hours recorded in radar after the transit of IGW on 15th January 2022. Amplitude scintillation and quasi- periodic oscillation in total electron content (TEC) were evident during the period [27]. It was discovered that the eruption's internal gravity waves had a considerable influence on surface pressure, causing both increases and decreases at the observation point. When compared to other settings, the

spread-F abnormalities caused by weaker atmospheric forcing were larger and lasted longer. ACARR's 205 MHz VHF radar proved useful in observing ionospheric abnormalities produced by the eruption. In the Indian EIA sector, plasma blob-like abnormalities and density depletions were discovered, indicating the propagation of internal

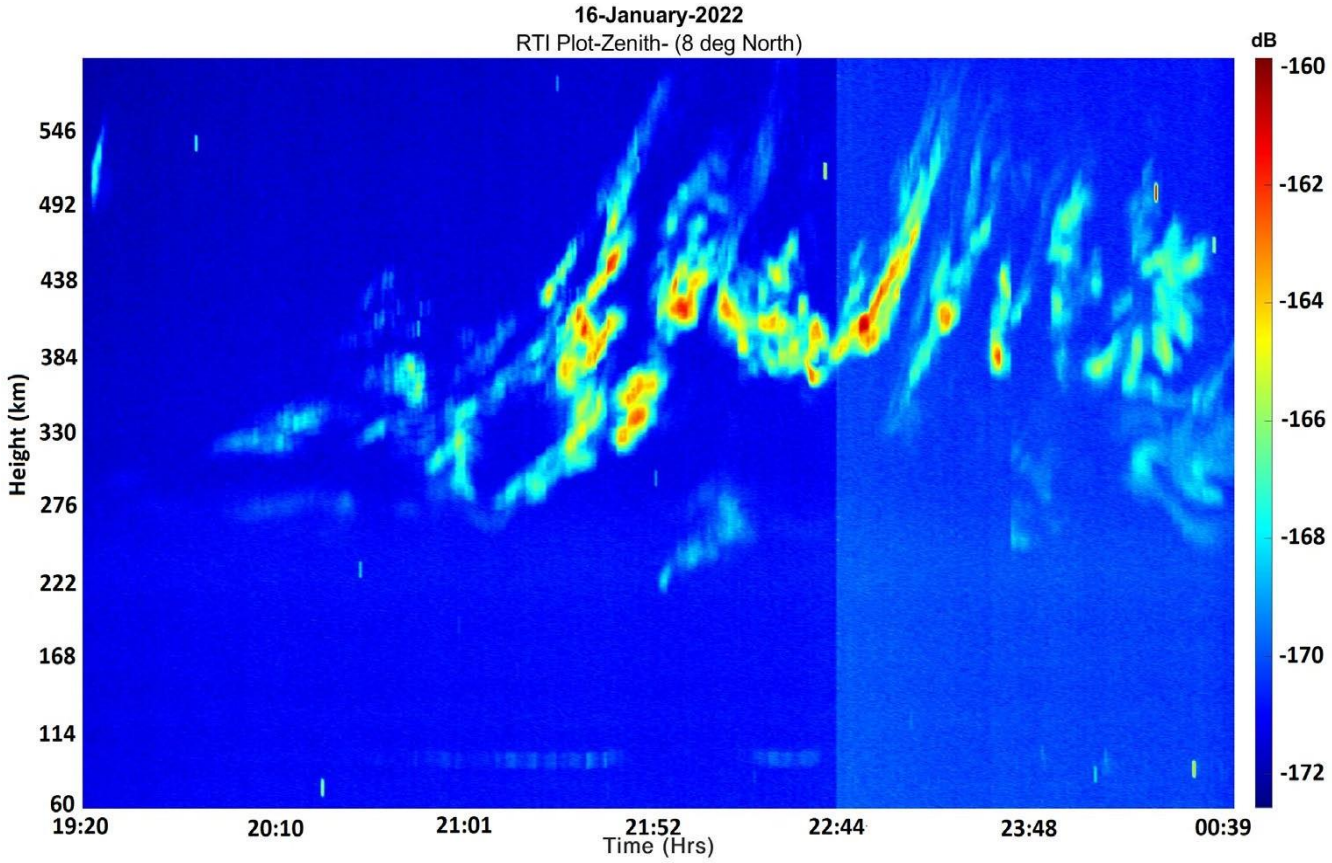

Figure 16: Night-time observation of F-region ionospheric irregularities during the Tonga volcanic eruption and associated Tsunami on 15th January 2022(Rakesh et.al.,2022).

gravity waves. The work emphasises the link between the lower atmosphere and the ionosphere and provides vital insights into the impacts of atmospheric-ionospheric coupling.

Geomagnetic storms in the early months of 2021 induced ionospheric perturbations.ST Radar was able to capture the event and pointed out the equatorward and poleward traverse of equatorial ionization anomaly (EIA) [28]. Article summarizes the ionospheric effects over Indian near-equatorial stations, Cochin and Changanacherry, during moderate and weak geomagnetic storms. The electron density profile shows inhibition of the Equatorial Ionization Anomaly (EIA) and a shift in its crest towards the equator. The Poleward Plasma Electric Field (PPEF) enhances the upward E×B drift, causing intermittent TEC depletions at the near equator. The storm-induced neutral winds establish the Disturbance Dynamo Electric Field (DDEF), causing long-term upward gradient drift instability and Equatorial Spread F (ESF) over Cochin. The combined effects of PPEF, DDEF, and Pre-Reversal Enhancement (PRE) lead to a major positive storm enhancement in TEC over Cochin.Shown in fig 17. Premonsoon thunderstorm day's atmospheric thermodynamics and the transition period from premonsoon to monsoon at Cochin were analyzed using radar, microwave radiometer, radiosonde, and automatic weather station. It is observed that boundary-layer and middle-layer moisture contents increase sharply, as well as abrupt changes in mixing height, lifting condensation level (LCL), convective available potential energy (CAPE), and other thermodynamic variables. Variations in Wet bulb Zero level (WBZ) were also noted during the period, an indicator of the onset of monsoon [29].

Cyclonic Storm Gaja landfall on 16th November 2018 in the south India Peninsula. The weak system intensified to cyclone in the Bay of Bengal, traversing through the Indian subcontinent survived to reach the Arabian Sea. Passage of cyclonic storm Gaja and its effect on troposphere circulation were observed using ST Radar. Its results were quite prominent upto 13 Km in height and atmosphere gravity waves were generated due to sudden

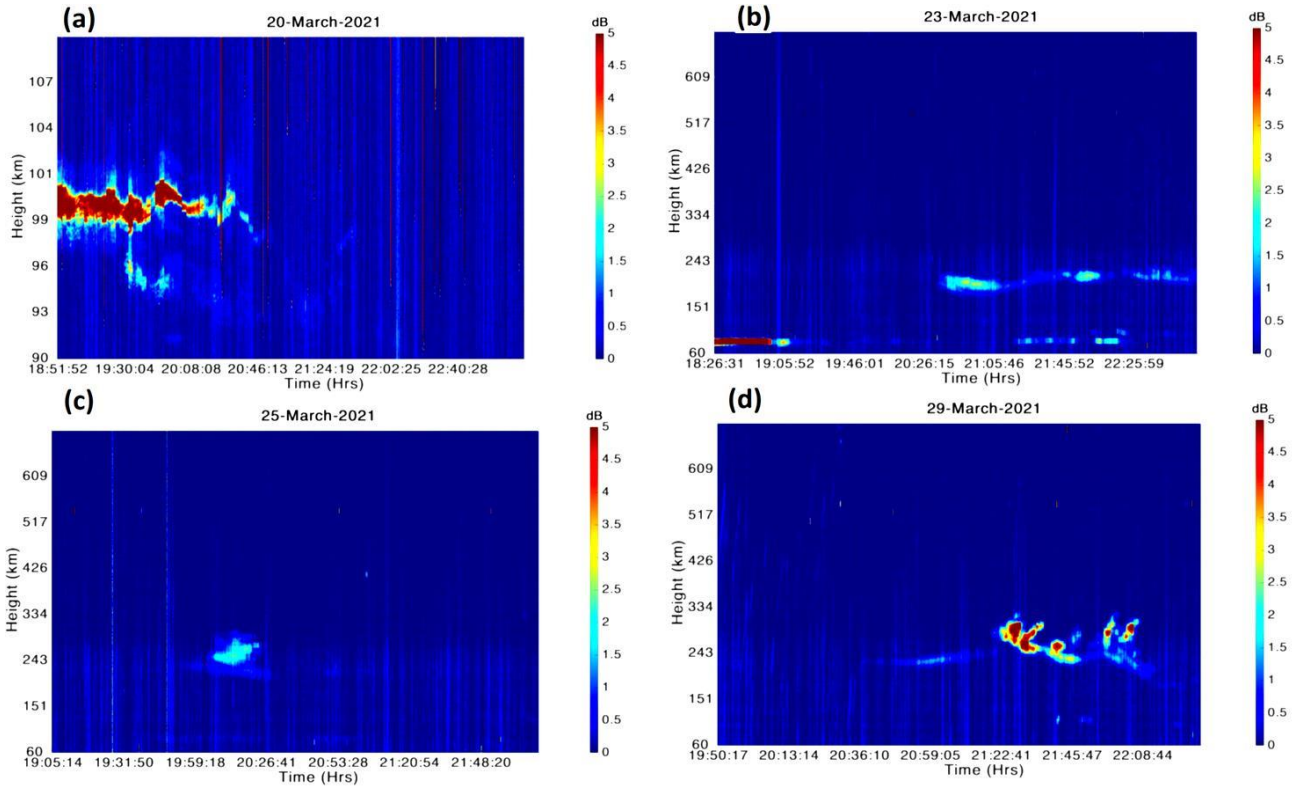

Figure 17: During the intense storm event 19 - 29 March 2021, an E-region irregularity echo was observed over Cochin on (a) 20 March 2021, and F-region irregularity echoes were observed on (b) 23 March 2021 (c) 25 March 2021 and (d) 29 March (Rakesh et al. 2019).

changes in topographical conditions. Abrupt disruption in tropospheric levels associated with the vertical distribution of turbulent kinetic energy was evident during Gaja cyclone [30].

High resolution of ST Radar's spectral width was used to study the diurnal variation of eddy dissipation rate. The study showed that the rate was increasing during afternoon hours, and at the boundary layer, convection increased the rate [31]. Inertial gravity waves (IGW) characteristics at the lower stratosphere/upper troposphere (UTLS) were observed using the wind profiler. Wavelengths of the waves were 3.74 and 1221 km vertically and horizontally, respectively. In conjunction with persistent deep depression, the upward transfer of energy from the upper troposphere to the lower stratosphere is also noted [32].

Tropopause height can be computed from radar's Signal to Noise ratio (SNR) profiles. Variability of cold point tropopause (CPT) height and factors responsible for the same have been explored. The correlation between tropical easterly jets and CPT was also investigated [33]. High- resolution data of UTLS from radar have been used to study about the exchange of water vapor, momentum, and energy between these layers. The study also indicates the stratosphere water vapour, and its unevenness can lead to climate change [34]. Interactions between stratosphere and troposphere during a pre-monsoon thunderstorm have been studied. During the event, strong convection reached the tropopause height, and considerable mixing has been observed [35].

Pre-monsoon and monsoon vertical structures of wind were investigated using radar wind profiles. As manifested by the development of monsoon circulations in the lower and upper troposphere, radar observations capture the gradual transition from pre-monsoon to monsoon season. It has been demonstrated that parameters describing the strength of monsoon circulations can be used as objective predictors of monsoon onset in Kerala [36].During the northeast monsoon (NEM) seasons of 2019 (excess) and 2020 (deficit), rainfall was contrasting in amount and pattern. With aid of

reanalysis data and wind profiler data study has been carried out by analysing atmospheric circulation pattern and its interaction with warm ocean waters to know more about the NEM contrast [37]. European Space Agency's unique and novel Aeolus wind measurement satellite provides real-time wind profiles from the surface up to 30 kilometres above the surface. Validation of the same was done with radar wind data and the Pearson correlation coefficient was near to 0.93[38].

5.1 Data Accessibility and Sharing

The Data Sharing Policy Terms & Conditions of the Advanced Centre for Atmospheric Radar Research (ACARR) state that data can be shared with other partners or public organizations/institutions under certain conditions. To request data, a formal letter must be submitted to the Director of ACARR, along with a consent form stating that the data will not be shared with third parties. Recipients are not allowed to claim any Intellectual Property rights related to the data without prior written consent. Access to the data is limited to qualified researchers from universities, organizations, and institutions, and sharing is based on merit and research objectives. The data is provided free of charge, but acknowledgment of the ACARR's contribution is required in any publication. Data will be shared after a minimum period of six months from the date of archival. By using the ACARR service, users accept the Data Fair Use Policy, which can be modified at any time. Data requests should include details of the requestor and the research objectives, collaborators, sponsors, and institutions involved.

6. Summary

Stratosphere-Troposphere (ST) wind profiler radar installed at Cochin, India, is a clear-air VHF Doppler radar system designed for continuous measurements of wind velocity under all weather conditions. World's first stratosphere-troposphere wind profiler radar at 205 MHz has been installed to measure wind profiles in the height range of 315 m-20 km. This radar is made up of 619 three-element Yagi-Uda antennas, each with a peak power aperture product of 1.6 x 108 Wm2. We offer a few of the results in this study to emphasise the radar's technical description, validation, and, most importantly, its numerous scientific applications. With a correlation of 0.99 for zonal wind and 0.93 for meridional wind, the radar wind measurements correlate quite well with the collocated radiosonde readings. The radar's accuracy in measuring zonal wind is found to be 1.85 m s-1 in zonal wind and 1.66 ms−1 in meridional wind.

The installation of this radar at Cochin is initially driven by the fact that, the southwest monsoon enters the Indian main land through this southwest coast and identified as the potential site to investigate the dynamics of the Indian summer monsoon. This facility is expected to produce a number of research results in the future. Continuous observation of monsoon circulation features over several years is expected to improve our understanding on tropical monsoon system and provides new insight to derive stronger predictors for forecasting monsoon variability. Furthermore, this radar's electronic beam steering capability can be used to analyse atmospheric dynamics such as deriving horizontal wind gradients, divergence, and so on. As stated in the introduction, the radar's unique location in Cochin, a place tucked between the Arabian Sea and the Western Ghats, aids in the research of gravity waves generated by mountains and tropical storms. Because the radar collects data from the lower stratosphere, it is feasible to analyse stratosphere-troposphere exchange processes that occur mostly during deep convective processes.

This radar's high-vertical-resolution observations (45 m) aid in the study of turbulence by allowing turbulent layers to be better defined and to explore more process level understanding. One of the radar's major features is its ability to distinguish rain echoes from background wind, which will be critical for studying the microphysical aspects of tropical rain-bearing clouds in the coming years. This radar can provide a more accurate depiction of the evolution of tropical thunderstorms. The radar is expected to last 25-30 years and offers important contributions to climate change research.

In summary, encouraging results from this radar are anticipated to increase our knowledge of monsoon dynamics, stratosphere-troposphere exchange

mechanisms, and turbulence. They also support local weather research and forecasting.

Acknowledgements

We would like to express our sincere thanks to the Ministry of Earth Sciences (MoES), Government of India, for supporting the ST Radar Facility at ACARR, CUSAT. We sincerely acknowledge and thank the Science and Engineering Research Board (SERB), Department of Science and Technology (DST), Government of India for providing the grant and for their assistance in the design and conception of the ST-radar facility at CUSAT.

References

Fukao S, Hamazu K. Radar for Meteorological and Atmospheric Observations; 2013.

Rottger J. Reflection and scattering of VHF radar signals from atmospheric refractivity structures. Radio Science. 1980;15(2):259–276. Available from: https://agupubs.onlinelibrary.wiley.com/doi/abs/10.1029/RS015i002p00259.

Hardy KR, Gage KS. The History of Radar Studies of the Clear Atmosphere. Atlas D, editor. Boston, MA: American Meteorological Society; 1990. Available from: https://doi.org/10.1007/978-1-935704- 15-7 17.

Hocking WK, Rottger J, Palmer RD, et al. The history of radar in atmospheric investigations; 2016.

Balsley BB, Gage KS. On the Use of Radars for Operational Wind Profiling. Bulletin of the American Meteorological Society. 1982;63:1009–1018.

Radar observation of the atmosphere. L. J. Battan (The University of Chicago Press) 1973. PP X, 324; 125 figures, 21 tables. £7•15. Quarterly Journal of the Royal Meteorological Society. 1973;99(422):793–793. Available from: https://rmets.onlinelibrary.wiley.com/doi/abs/10.1002/qj.49709942229.

Chadwick RB. A feasibility study on using wind profilers to support space shuttle launches. NASA: NASA; 1984. Report 3861.

Mohanakumar K, Kottayil A, Anandan VK, et al. Technical Details of a Novel Wind Profiler Radar at 205 MHz. Journal of Atmospheric and Oceanic Technology. 2017;34:2659–2671.

Turtle AJ, Baldwin JE. A Survey of Galactic Radiation at 178 Mc/s. Monthly Notices of the Royal Astronomical Society.1962 06;124(6):459–476. Available from: https://doi.org/10.1093/mnras/124.6.459.

Ben-yosef N, Tirosh E, Weitz A, et al. Refractive-index structure constant dependence on height. Journal of the Optical Society of America. 1979;69:1616–1618.

Titu Samson PM. Design development calibration and validation of 205 MHz wind profiler radar [dissertation]. Cochin University of Science and Technology. Kerala India; 2020.

Balsley BB. In: Atlas D, editor. Clear-Air Radar Technology: Panel Report. Boston, MA: American Meteorological Society; 1990. p. 282–286. Available from: https://doi.org/10.1007/978-1-935704-15-7 24.

Samson TK, Kottayil A, Manoj MG, et al. Technical Aspects of 205 MHz VHF Mini Wind Profiler Radar for Tropospheric Probing. IEEE Geoscience and Remote Sensing Letters. 2016;13(7):1027– 1031.

Samson TK, Babu B, Anandan VK, et al. Phased array of 619-element Yagi- Uda antenna for Wind Profiler Radar at Cochin University of Science and Technology. In: 2019 URSI Asia-Pacific Radio Science Conference (APRASC); 2019. p. 1–4.

Balanis CA. Antenna theory: analysis and design. Wiley-Interscience; 2005.

Frank Gekat* RH Peter G¨olz. Weather Radar Calibration and Testing using the Moon as Reference Target. 2011 09; Available from: https://ams.confex.com/ams/35Radar/webprogram/Paper191872.html.

Kottayil A, Mohanakumar K, Samson T, et al. Validation of 205 MHz wind profiler radar located

at Cochin, India, using radiosonde wind measurements. Radio Science. 2016;51(3):106–117.

Mohanakumar K, Santosh K R, Mohanan P, et al. A Versatile 205 MHz Stratosphere– Troposphere Radar at Cochin – Scientific Applications. Current Science. 2018.

Pattanaik DR, Satyan V. Fluctuations of Tropical Easterly Jet during contrasting monsoons over India: A GCM study. Meteorology and Atmospheric Physics. 2000; 75:51–60.

Narayanan S, Kottayil A, Mohanakumar K. Monsoon low-level jet over the gateway of Indian summer monsoon: a comparative study for two distinct monsoon years. Meteorology and Atmospheric Physics. 2016 12;128.

Kottayil A, Xavier P, Satheesan K, et al. Vertical structure, and evolution of monsoon circulation as observed by 205-MHz wind profiler radar. Meteorology and Atmospheric Physics. 2019; 132:531– 545.

M. G. Manoj, S. C., R. V., R. Rebello, A. S., and M. K, "Atmospheric response to the annular solar eclipse of 26 December 2019 over Cochin, India," Adv. Space Res., vol. 68, no. 9, pp. 3610–3621, Nov. 2021, doi: 10.1016/j.asr.2021.07.001.

R. Remya, M. G. Manoj, V. Rakesh, K. Mohanakumar, and C. Sivan, "Influence of High Latitude Sudden Stratospheric Warming on Tropical Weather: Observations From a 205 MHz Stratosphere Troposphere Radar and Surface Meteorological Parameters," Earth Space Sci., vol. 8, no. 4, p. e2020EA001418, 2021, doi: 10.1029/2020EA001418.

M. G. Manoj, Mohankumar, V. Rakesh, and R. Rebello, "Features of low level winds over Cochin during the deluge of Monsoon-2018 using 205 MHz wind Profiler Radar," in 2019 URSI Asia-Pacific Radio Science Conference (AP-RASC), Mar. 2019, pp. 1–2. doi: 10.23919/URSIAP-RASC.2019.8738657.

M. C. Neethu Mohan et al., "Potential Application of 205-MHz Stratosphere–Troposphere Wind Profiling Radar in Ionospheric Studies: Preliminary Results," IEEE Geosci. Remote Sens. Lett., vol. 17, no. 6, pp. 918–922, Jun. 2020, doi: 10.1109/LGRS.2019.2938855.

Rakesh. V., M. G. Manoj, K. Mohankumar, M. Neethu, and T. K. Samson, "Detection of Submeter Scale Irregularities in the Low-Latitude Ionospheric E Layer Using High VHF Radar at 205 MHz," J. Geophys. Res. Space Phys., vol. 124, no. 5, pp. 3752–3760, May 2019, doi: 10.1029/2018JA026302.

V. Rakesh et al., "Impact of the Hunga Tonga-Hunga Ha'apai volcanic eruption on the changes observed over the Indian near-equatorial ionosphere," Adv. Space Res., vol. 70, no. 8, pp. 2480–2493, Oct. 2022, doi: 10.1016/j.asr.2022.07.004.

S. Haridas et al., "Geomagnetic storm-induced perturbations over Indian equatorial ionosphere," Adv. Space Res., Apr. 2023, doi: 10.1016/j.asr.2023.04.017.

T. Anna Mathew et al., "Pre-monsoon convective events and thermodynamic features of southwest monsoon onset over Kerala, India – A case study," Atmospheric Res., vol. 248, p. 105218, Jan. 2021, doi: 10.1016/j.atmosres.2020.105218.

C. Sivan, V. Rakesh, M. G. Manoj, K. Satheesan, S. Abhilash, and K. Mohanakumar, "Detection of the impact of a tropical cyclonic system on the dynamics and energetics of the atmosphere using wind profiler radar," J. Atmospheric Sol.-Terr. Phys., vol. 235, p. 105896, Sep. 2022, doi: 10.1016/j.jastp.2022.105896.

S. K. Raghavan and A. Kottayil, "Diurnal Variation of Turbulent Eddy Dissipation Rate Studied using 205 MHz Wind Profiler Radar," presented at the 38th Conference on Radar Meteorology, AMS, Aug. 2017. Accessed: Jul. 02, 2023. [Online]. Available: https://ams.confex.com/ams/38RADAR/meetingapp.cgi/Paper/321134

A. Kottayil, K. Satheesan, K. Mohankumar, S. Chandran, and T. Samson, "An investigation into

the characteristics of inertia gravity waves in the upper troposphere/lower stratosphere using a 205 MHz wind profiling radar," Remote Sens. Lett., vol. 9, no. 3, pp. 284–293, Mar. 2018, doi: 10.1080/2150704X.2017.1418991.

K. Nithya, A. Kottayil, and K. Mohanakumar, "Determining the tropopause height from 205 MHz stratosphere troposphere wind profiler radar and study the factors affecting its variability during monsoon," J. Atmospheric Sol.-Terr. Phys., vol. 182, pp. 79–84, Jan. 2019, doi: 10.1016/j.jastp.2018.10.018.

S. P. Sujithlal, K. Satheesan, A. Kottayil, and K. Mohankumar, "Thunderstorm induced stratosphere-troposphere exchange during pre-monsoon over Kochi," in 2019 URSI Asia-Pacific Radio Science Conference (AP-RASC), Mar. 2019, pp. 1–1. doi: 10.23919/URSIAP-RASC.2019.8738476.

S. P. Sujithlal, K. Satheesan, A. Kottayil, and K. Mohanakumar, "Observation of stratosphere–troposphere exchange during a pre-monsoon thunderstorm activity over Kochi, India," Meteorol. Atmospheric Phys., vol. 134, no. 3, p. 53, May 2022, doi: 10.1007/s00703-022-00893-7.

A. Kottayil, P. Xavier, K. Satheesan, K. Mohanakumar, and V. Rakesh, "Vertical structure and evolution of monsoon circulation as observed by 205-MHz wind profiler radar," Meteorology. Atmospheric Phys., vol. 132, no. 4, pp. 531–545, Aug. 2020, doi: 10.1007/s00703-019-00695-4.

S. Sankar et al., "Contrasting features of northeast monsoon during 2019 and 2020 in response to the delayed withdrawal of southwest monsoon," Theor. Appl. Climatology., vol. 153, no. 1, pp. 19–34, Jul. 2023, doi: 10.1007/s00704-023-04467-4.

A. Kottayil et al., "Assessing the quality of Aeolus wind over a tropical location (10.04 N, 76.9 E) using 205 MHz wind profiler radar," Int. J. Remote Sens., vol. 43, no. 9, pp. 3320–3335, May 2022, doi: 10.1080/01431161.2022.2090871.

Fukao, S., K. Wakasugi, T. Sato, S. Morimoto, T. Tsuda, I. Hirota, I. Kimura, and S. Kato, 1985: Direct measurement of air and precipitation particle motion by very high frequency Doppler radar. Nature, 316, 712–714, https://doi.org/10.1038/316712a0.

Martin Ralph, F., 1995: Using radar-measured radial vertical velocities to distinguish precipitation scattering from clear-air scattering. J. Atmos. Oceanic Technol., 12, 257, https://doi.org/10.1175/1520-0426(1995)012<0257:URMRVV>2.0.CO;2.

D. R, A. Pradeep, A. S and M. P, "Performance Comparison of Adaptive Algorithms in Identifying Clear Air and Rain Echoes in the 205 MHz-ST Radar Framework," 2021 8th International Conference on Smart Computing and Communications (ICSCC), Kochi, Kerala, India, 2021, pp. 90-93, doi: 10.1109/ICSCC51209.2021.9528145.

R. Dhanya, A. Pradeep, C. S. Abhiram Nirmal, S. Abhilash, K. Mohankumar and P. Mohanan, "A Novel Hybrid Approach for the Identification of Clear Air and Rain Echoes in the 205 MHz ST Radar Spectrum," in IEEE Geoscience and Remote Sensing Letters, vol. 19, pp. 1-5, 2022, Art no. 4022105, doi: 10.1109/LGRS.2022.3149149.